Available online at www.sciencedirect.com
SCIENCE DIRECT
Polymer 46 (2005) 1893–1898
polymer
www.elsevier.com/locate/polymer

# Diffusional behavior of multi-arm star polymers by $^1$H pulsed field gradient spin-echo NMR method

Taiichi Furukawa[a,*], Koji Ishizu[a], Yuji Yamane[b], Isao Ando[b]

[a]*Department of Organic Materials and Macromolecules, International Research Center of Polymer Science, Tokyo Institute of Technology, 2-12-1-H133, Ookayama, Meguro-ku Tokyo 152-8552, Japan*
[b]*Department of Chemistry and Materials, Tokyo Institute of Technology, International Research Center of Macromolecular Science, 2-12-1 Ookayama, Meguro-ku Tokyo 152-8552, Japan*

Received 12 October 2004; received in revised form 6 December 2004; accepted 17 December 2004
Available online 19 January 2005

**Abstract**

The diffusional behavior of multi-arm star-shaped p(*t*BMA) was investigated in a concentration range from dilute to semidilute region with $^1$H pulsed field gradient spin-echo NMR (PFGSE-NMR). An 142-arm star-shaped p(*t*BMA) showed two diffusional mode, which reflected the coexistence of liquid ordering phase and liquid phase near the ordering transition. On the other hand, for star-shaped p(*t*BMA) with 55 arms showed a single diffusional relaxation in all concentration ranges during observation time. In the semidilute region, the relationship between the diffusion coefficient against the polymer concentration was affected strongly not only the arm number but also liquid ordering structure.


*Keywords:* Soft sphere; Diffusional behavior; Ordering

## 1. Introduction

Star-branched polymers are characterized as structures where all the chains of a molecule are linked together to a small-molar-mass core. Generally, star polymers exhibit smaller hydrodynamic dimensions than the linear polymer with identical molar mass. The interest in star polymers arises not only from the fact that they are models for branched polymers but also from their enhanced segment densities. Zimm and Stockmayer were the first to study the conformation of star-branched polymers using classical theories [1]. Daoud and Cotton studied the conformation and dimensions of star polymers using scaling theories [2]. Several groups have reported that the conformation of star polymer in good solvent was in agreement with the Daoud–Cotton scaling model of stars. Their dilute-solution properties suggested that they behaved not as hard spheres but as soft spheres [3].

Stars with multiarms (the critical number of arms is estimated to be of order $10^2$) are expected to form a crystalline array near the overlap threshold ($C^*$) by Witten et al. [4]. We investigated in detail the structural ordering of stars by means of small-angle X-ray scattering (SAXS) [5]. Polyisoprene (PI) stars (arm number $f >$ ca. 90) formed a body-centered-cubic (bcc) structure near $C^*$. This structure changed to a mixed lattice of bcc and face-centered-cubic (fcc) structures with increasing polymer concentration. Recently, we also synthesized functionalized poly(ethylene oxide) (PEO) stars possessing a tertiary amino group at each arm end. Subsequently, positive charges were introduced into such peripheral tertiary amino groups by quarternization with methyl iodide ($CH_3I$). It was found that these peripherally charged stars ($f > 37$) formed a lattice of BCC below $C^*$ due to the electrostatic repulsion between stars [6].

Self-diffusion of several linear polymers in dilute, [7–9] concentrated solutions, [8–11] and in the melt [7,11–13] has been measured. The results were interpreted as consistent with the reptation concept [8,9,14]. Much less work has been performed, however, on the diffusional behavior of star

* Corresponding author. Tel.: +81 3 5734 2634; fax: +81 3 5734 2888.
*E-mail address:* tfurukaw@polymer.titech.ac.jp (T. Furukawa).

0032-3861/$ - see front matter © 2005 Elsevier Ltd. All rights reserved.
doi:10.1016/j.polymer.2004.12.054

polymer solutions. A few reports are relatively limited by small arm numbers. Meerwall et al. indicated that molecular motions for PI stars with $f=3$, 8, and 18 were not qualitatively different from those of linear polymers at any concentration, including the melt [15,16].

In this article, we investigated the diffusional behavior of multi-arm stars ($f=55$ and 142) through $^1$H pulsed field gradient spin-echo (PFGSE-NMR) measurement. The correlation between the structural ordering and the diffusional behavior was discussed in details.

## 2. Experimental

### 2.1. Materials

Star-shaped p(*t*BMA)s were synthesized by polymerization of p(*t*BMA) macroinitiator with ethylene glycol dimethacrylate (EGDMA) with CuBr complexed by PMDETA (*N*,*N*,*N*′,*N*″,*N*″-pentamethyldiethylenetriamine) as the catalyst in toluene at 80 °C. Subsequenly, the reaction solvent was changed to THF after removing toluene using a rotary evaporator and was precipitated in methanol/$H_2O$ (7/3 v/v) after passing through an alumina column to remove the copper complexes. Unreacted p(*t*BMA) was removed from the polymerization products by the precipitation fractionation with a THF-methanol/$H_2O$ system. Details concerning the synthesis of such star-shaped p(*t*BMA) have been given elsewhere [17].

The weight-average molecular weight ($M_w$) of the fractionated star-shaped p(*t*BMA) was determined by static light scattering (SLS: Photal TMLS-6000HL: Otsuka Electronics, $\lambda_0=632.8$ nm) in THF at 25 °C with Zimm mode. The scattering angle was in the range 30–150°. The RI increment d*n*/d*c* (=0.04 mL/g in THF) of star-shaped p(*t*BMA) was measured with a differential refractometer (Photal DRM-1021: Otsuka Electronics). Sample solutions were filtered through membrane filters with a nominal pore of 0.2 μm just before measurement.

The diffusion coefficient ($D_0$) was determined by the extrapolation to zero concentration on dynamic light scattering (DLS: Otsuka Electronics) data with Cumulant method at 25 °C in THF. The scattering angle was 90°.

### 2.2. SAXS measurement

The SAXS intensity distribution was measured with a rotating-angle X-ray generation (Rigaku Denshi Rotaflex RTP 300RC) operated at 40 kV and 100 mA. The X-ray source was monochromatized to Cu $K_\alpha$ ($\lambda=1.5418$ Å) radiation. In the measurement of the solution sample, a glass capillary ($\phi=2.0$ mm, Mark-Röhrchen Ltd) was used as a holder vessel. The SAXS patterns were taken with a fine-focused X-ray source using a flat plate camera (Rigaku Denki, RU-100). The SAXS intensity profiles plotted from the horizontal section of the SAXS patterns without considering the smearing correction.

### 2.3. PFGSE-NMR measurement

The self-diffusion coefficient ($D$) measurements of star-shaped p(*t*BMA) were carried out by means of a Bruker DSX-300 NMR spectrometer operating at 300.1 MHz for $^1$H at 25 °C with a homemade pulse gradient generator. The homemade pulse gradient generator is designed to generate a strong field gradient pulse (with the maximum field strength of about 1100 G cm$^{-1}$) and to suppress the eddy currents induced. The spectral width and number of data points were 4.0 kHz and 4096, respectively. Only the free induction decay (FID) was recorded after the echo maximum and then the Fourier transformation (FT) was applied.

The $D$ values were determined by using the relationship between echo signal intensity and field gradient parameters:

$$\ln\left[\frac{A(2\tau)}{A(0)}\right] = -\gamma^2 G^2 D\delta^2\left(\Delta-\frac{\delta}{3}\right) \tag{1}$$

where $A(2\tau)$ and $A(0)$ are the echo signal intensities at $t=2\tau$ with and without the magnetic field gradient pulse strength $G$ with has the length $\delta$, respectively. $\gamma$ is the gyromagnetic ratio of the proton and $\Delta$ is the gradient pulse interval. The echo signal intensity was measured as a function of $G$. Plots of $\ln[A(2\tau)/A(0)]$ against $\gamma^2G^2\delta^2(\Delta-\delta/3)$ give a straight line with a slope of $-D$. Therefore, the $D$ value can be determined from its slope. When stars have two components in diffusion on the measurement time scale, the total echo attenuation is given by a superposition of contributions from the individual components as expressed by:

$$\frac{A(2\tau)}{A(0)} = p_1\exp\left[-\gamma^2G^2D_1\delta^2\left(\Delta-\frac{\delta}{3}\right)\right] + p_2\exp\left[-\gamma^2G^2D_2\delta^2\left(\Delta-\frac{\delta}{3}\right)\right] \tag{2}$$

where $D_i$ is the self-diffusion coefficient of the $i$th component, and $p_i$ is the fraction of the $i$th component and thus $p_1+p_2=1$. The fraction for the fast and slow diffusion components can be determined from the intercept of the least-squares fitted straight line.

## 3. Results and discussion

### 3.1. Dilute-solution properties of star-shaped p(tBMA)

In previous report [17], we prepared star-shaped p(*t*BMA) were synthesized by polymerization of p(*t*BMA) macroinitiator with EGDMA with CuBr complexed by PMDETA as the catalyst in toluene at 80 °C. Subsequently, we examined the dilute-solution properties of stars using

SLS and DLS in THF at 25 °C. The observed physical values are quoted from Ref. [17] (Table 1). In this table, the sample code $(SB20)_{142}F$ means $M_w$ of arm $= 2.0 \times 10^4$ and arm number = 142.

The dynamics of star-shaped p(*t*BMA) in dilute solution can be analyzed by DLS. Here, we define the normalized first-order correlation function for the scattered electric field $g^{(1)}(\tau)$ from the sample, where $\tau$ is time. In a DLS measurement, we obtain the second-order correlation function, $g^{(2)}(\tau)$. The two correlation functions are linked via the Siegert relation:

$$g^{(2)} = 1 + |g^{(1)}(\tau)|^2 \quad (3)$$

If the scattering medium has only one relaxation modes, $g^{(2)}(\tau) - 1$, is simply given one exponential functions. Fig. 1 shows an example of the correlation function for $(SB20)_{142}F$ in THF (concentration 0.1 wt%). In this dilute region, the correlation function shows existence of single relaxation corresponding to the translational diffusion of individual stars. The result of DLS data obtained for star-shaped $(SB14)_{55}F$ was the same as that for the star-shaped $(SB14)_{142}F$. The translational diffusion coefficient $D_0$ can be estimated by extrapolation of polymer concentration to zero. The hydrodynamic radius ($R_H$) can be estimated by the Stokes Einstein's equation $R_H = kT/6\pi\eta_0 D_0$, where $k$, $T$, and $\eta_0$ indicate Boltzmann coefficient, absolute temperature, and viscosity of solvent, respectively. The ratio $R_G/R_H$ is a sensitive fingerprint of the inner density profile of star molecules and polymer micelles. The values of $R_G/R_H$ for stars were in the range of 1.16–1.22. It is well known that $R_G/R_H$ for unperturbed polymers and hard spheres with uniform density are 1.25–1.37 [18] and 0.775 [19], respectively. It is concluded that star-shaped p(*t*BMA)s show a single relaxation process and behave not as hard spheres but as soft spheres in dilute solution.

### 3.2. Structural ordering of stars

According to the theoretical studies, the ordering phenomena should appear near the overlap threshold ($C^*$) [4]. Thus, we examined the structural ordering of stars by means of SAXS in toluene. Fig. 2 shows SAXS intensity profiles for $(SB14)_{55}F$ at 25 wt% and for $(SB20)_{142}F$ at 15 wt%, where $q[=(4\pi/\lambda)\sin\theta]$ (where $\theta$ is one-half the scattering angle) is the magnitude of the scattering vector.

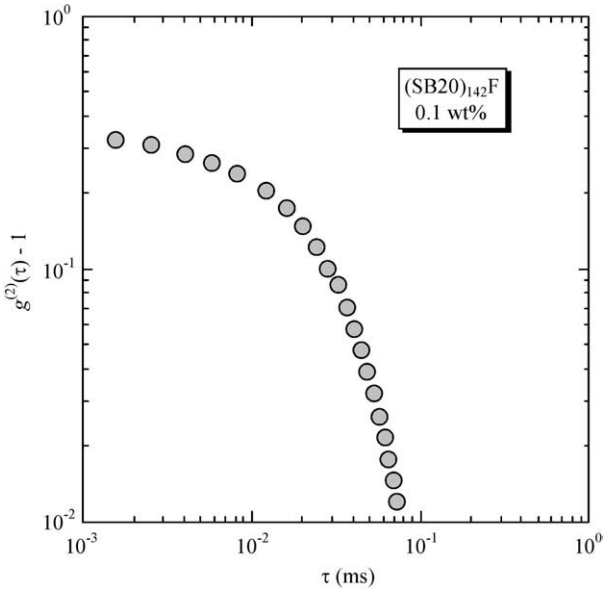


Fig. 1. The correlation function of for $(SB20)_{142}F$ in THF (concentration 0.1 wt%).

Each polymer concentration was higher than the $C^*$ (10.4 wt% for $(SB14)_{55}F$ and 12.4 wt% for $(SB20)_{142}F$). For $(SB14)_{55}F$, no regular scattering peaks appeared at this concentration due to disordering. On the other hand, for $(SB20)_{142}F$, the first four peaks appear closely at the relative $q$ positions of $1:\sqrt{2}:\sqrt{3}:\sqrt{4}$, as shown in parentheses. The interplanar spacing ($d_1/d_i$) at the scattering angles is relative to the angle of the first maximum according to Bragg's equation: $2d \sin\theta = n\lambda$ (where $\lambda = 1.5418$ Å). In general, this packing pattern appears in the lattice of not only simple cubic but also bcc structures. As mentioned in the Section 1, the stars with multiarm were packed in the lattice of a bcc structure near $C^*$ [5,6]. The conformation of star-shaped p(*t*BMA) can be regarded as similar to such star in solution. It is reasonable that these values corresponding to the packing pattern of (110), (200), (211), and (220) planes in a bcc structure.

### 3.3. Diffusional behavior of stars

We studied first the dependence of the diffusion coefficient of star-shaped p(*t*BMA) on the polymer concentration. As, Fig. 3 shows the plots of $\ln[A(2\tau)/A(0)]$ against $\gamma^2 G^2 \delta^2 (\Delta - \delta/3)$ for $(SB14)_{55}F$ in $CDCl_3$. It is

Table 1
Characteristics of star-shaped p(*t*BMA)

| Sample | $10^{-6}\,\bar{M}_w$ [a] | $M_w/M_n$ [b] | $f$ | $R_G$ [a] (nm) | $R_H$ [c] (nm) | $R_G/R_H$ | $C^*$ [d] (wt%) |
|---|---|---|---|---|---|---|---|
| $(SB14)_{55}F$ | 0.72 | 1.06 | 55 | 16.5 | 13.5 | 1.22 | 10.4 |
| $(SB20)_{142}F$ | 2.8 | 1.15 | 142 | 23.9 | 20.6 | 1.16 | 12.4 |

[a] Determined by SLS in THF.
[b] Determined by GPC using universal calibration.
[c] Determined by DLS in THF.
[d] Calculated by the equation: $C* = \frac{3\bar{M}_w}{4\pi R_H N_A}$.

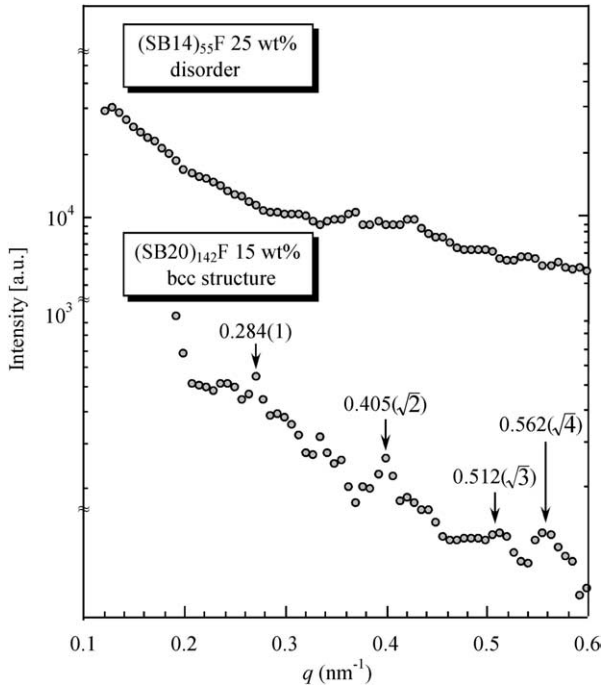


Fig. 2. SAXS intensity profiles: (a) $(SB14)_{55}F$ at 25 wt% (b) $(SB20)_{142}F$ at 15 wt%.

seen the experimental data lie on a straight line over a broad concentration range from dilute to semidilute. This means that star-shaped p(*t*BMA) with $f=55$ has a single-component of diffusion during the observation time.

Fig. 4 shows the dependence of diffusion coefficient on the normalized concentration $C/C^*$ for $(SB14)_{55}F$. It is found from this figure that the dependence of diffusion coefficient on the polymer concentration is divided into three regions. For $C/C^*<0.5$ (region I), the diffusion

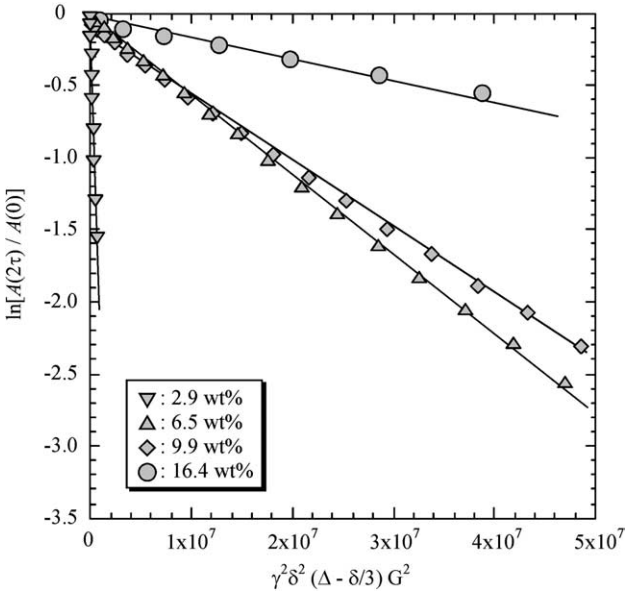


Fig. 3. Diffusional spin-echo attenuation of $(SB14)_{55}F$ in various concentration.

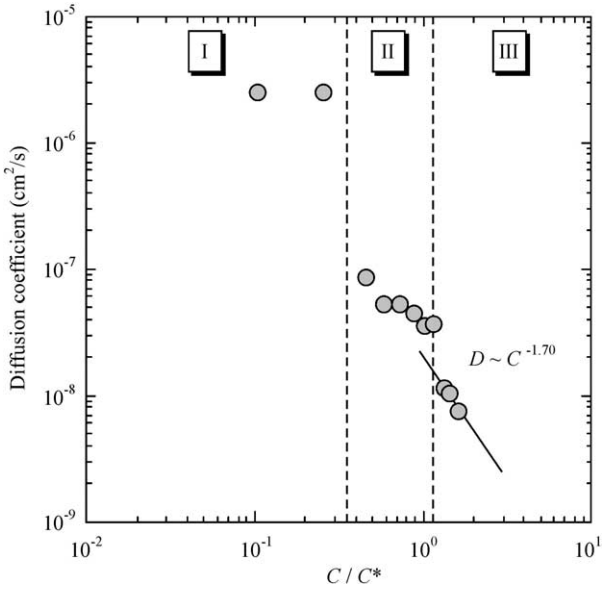


Fig. 4. The plot of the diffusion coefficient of $(SB14)_{55}F$ against the polymer concentration.

coefficient has almost same value ($D=2.5\times10^{-5}$ cm$^2$/s) corresponding to the self-diffusion of individual stars, which is in agreement with DLS data [17]. For $0.5<C/C^*<1$ (region II), the sudden decrease of the diffusion coefficient is observed. In this region, the interaction such as collision or repulsion between stars exists during the observation time. For $1<C/C^*$ (region III), the gradual decrease of the diffusion coefficient is observed. In this region, the diffusion coefficient is proportional to the -1.70th power of the polymer concentration. This data is agreement well with de Gennes' prediction [20] of a concentration scaling regime $D\sim C^{-1.75}$ $(1<C/C^*)$. This value, however, is suspect both because the semidilute solution scaling regime on which they are based could not be demonstrated experimentally and because the segmental motions of stars are probably beginning to contribute to the diffusion in this region. It should be noted that $C^*$ as defined here represents the concentration associated with the onset of screening the hydrodynamic interaction rather than the onset of entanglements, which should occur at a higher polymer concentration and accompanied with the molecular weight of arm. In our case, any scaling behavior observed in the semidilute region is probably unrelated not to reptation process but to the friction of the segmental motions.

The dependence of the diffusion coefficient of star-shaped p(*t*BMA) with $f=142$ on the polymer concentration is also investigated. As shown previous section, this star forms a bcc structure above $C^*$. Fig. 5 shows the plots of $\ln[A(2\tau)/A(0)]$ against $\gamma^2G^2\delta^2(\Delta-\delta/3)$ in $CDCl_3$ for $(SB20)_{142}F$. As shown in Fig. 5(a), for 2.5 wt% solution, the experimental data lie on a straight line. This means that the diffusion of stars is a single diffusional relaxation. In 6.2, 7.6, 9.6 wt% solutions, the plots of $\ln[A(2\tau)/A(0)]$ against $\gamma^2G^2\delta^2(\Delta-\delta/3)$ consist of two exponential decays as shown

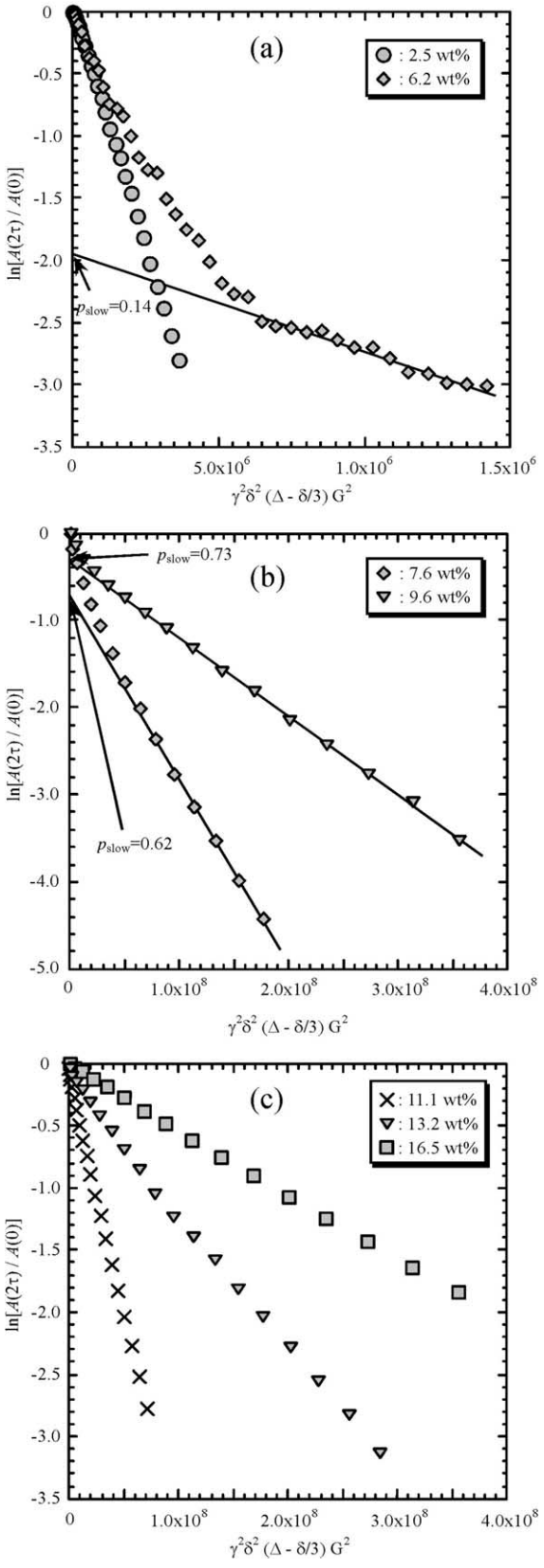


Fig. 5. Diffusional spin-echo attenuation of $(SB20)_{142}F$ in various concentration. The fraction for the slow diffusion component, $p_{slow}$, can be determined from the intercept of the least-squares fitted straight line.

in Fig. 5(a) and (b). This observation shows that the diffusion is made up of two kinds of diffusion components such as the fast diffusion component and the slow diffusion component. The fast diffusion component and the slow diffusion component in the two phases correspond to the diffusion of single star and the diffusion of liquid ordering phase. The fractions of the two kinds of diffusion components can be determined from the intercept of the least-squares fitted straight line as shown in Fig. 5(a) and (b). As for 6.2, 7.6, 9.6 wt% solutions, the fractions of the slow diffusion component are 0.14, 0.62, and 0.73, respectively. With increasing the polymer concentration, the fraction of the slow diffusion component increases and gradually reaches 1.0.

In 11.1, 13.2, 16.5 wt% solutions, which is in the bcc structure phase, the plots of $\ln[A(2\tau)/A(0)]$ against $\gamma^2G^2\delta^2(\Delta-\delta/3)$ become a straight line as shown Fig. 5(c). This result shows that the diffusion of stars is a single diffusion component again. The slope of the plots decreases with increasing the polymer concentration, which means slower diffusion coefficient.

Fig. 6 shows the dependence of diffusion coefficient on the normalized concentration $C/C^*$ for $(SB20)_{142}F$. It is found that the diffusional process is also classified into three region as well as $(SB14)_{55}F$. For $C/C^*<0.5$ (region I), a single diffusion component is observed, corresponding to the self-diffusion of individual stars. For $0.5<C/C^*<1$ (region II), a crossover transition from a single star to liquid ordering phase is observed. And, the diffusion coefficient suddenly decreases with increasing the polymer concentration. Although this sample shows the dynamic two-phase behavior, no visible macroscopic phase separation or optical inhomogeneity could be detected. For $1<C/C^*$ (region III), the gradual decrease of the diffusion coefficient is observed.

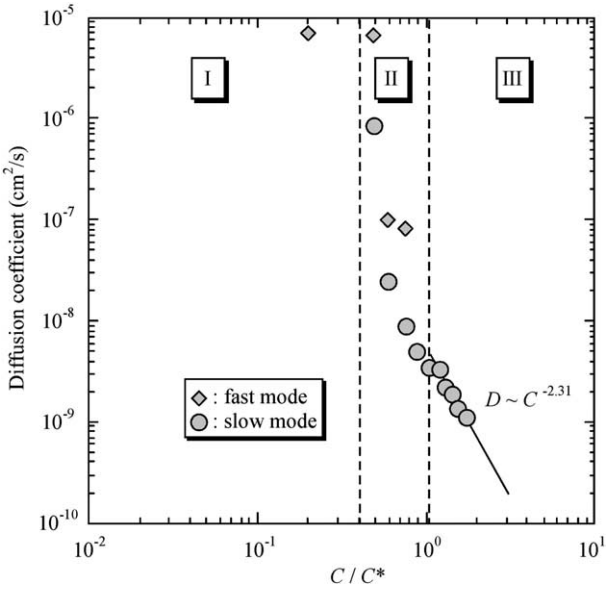


Fig. 6. The plot of the diffusion coefficient of $(SB20)_{142}F$ against the polymer concentration.

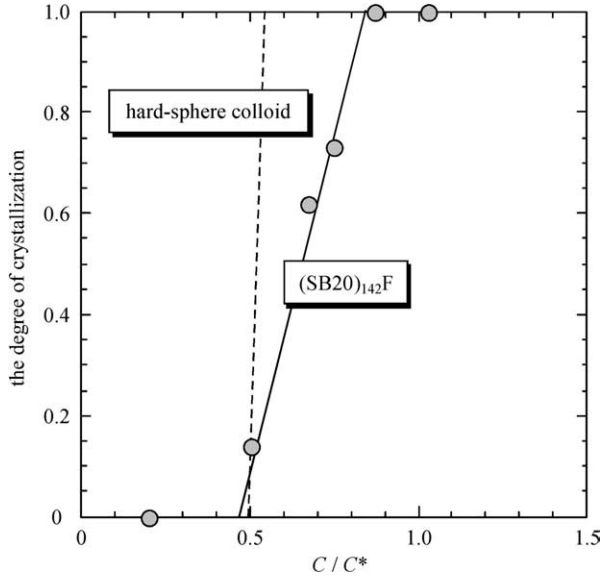


Fig. 7. The plots of the degree of the crystallization as a function of the normalized concentration $C/C^*$ for $(SB20)_{142}F$ and hard-sphere colloid.

In this region, the diffusion coefficient is proportional to the -2.31th power of the polymer concentration. This scaling value is larger than that of $(SB14)_{55}F$. The ordered multiarm stars are seen to interact between arms of neighbors' stars. Thus, the friction of the segment motion and the restricted motions of core of star probably reflect the larger scaling value. This similar observation is seen in the case of hard-sphere colloids [21] and diblock copolymers [22,23] in the ordering region, which show that the diffusion coefficient exhibits a slowing down due to the liquid like ordering.

Fig. 7 shows the plots of the degree of the crystallization as a function of the normalized concentration $C/C^*$ for $(SB20)_{142}F$ and hard-sphere colloid. Here, the degree of the crystallization is defined as the ratio of the slow diffusion component to the fast diffusion component. For hard-sphere colloidal particles with a low polydispersity, crystallization sets in at $\phi_{cr}=0.494$, and it is complete at $\phi_m=0.545$ [21, 24]. The onset of apparent crystallization is observed in our stars at $\phi_{cr}=(C/C^*)_{cr}=0.47$ with coexistence of a single molecule and liquid ordering phases until $\phi_m=0.84$. The diffusion coefficient in the coexisting liquid phase appears to be unaffected by the presence of the slow diffusion component, that is, the concentration in the liquid phase remains unchanged and only its fraction decreases until crystallization is complete. Compared with the result of hard-sphere colloid, the crystallization process of our stars is much slower. This difference could be due to the particle nature in solution, that is, our stars behave as soft sphere, while colloid particles behave as hard sphere in good solvent.

## 4. Conclusions

The diffusional behavior of multiarm star-shaped poly(*tert*-butyl methacrylate)s (p(*t*BMA)) was investigated in a concentration range from dilute to semidilute region with $^1H$ pulsed field gradient spin-echo NMR (PFGESE-NMR). A star-shaped p(*t*BMA) with 142 arms showed two diffusional mode, which reflected the coexistence of liquid ordering phase and liquid phase near the ordering transition. On the other hand, for p(*t*BMA) with 55 arms showed a single diffusional relaxation in all concentration ranges during observation time. In semidilute solution, the diffusion coefficient of a star-shaped p(*t*BMA) with 142 arms showed the larger dependence on the polymer concentration than that of a star-shaped p(*t*BMA) with 55 arms, which reflect the difference of the friction of the segment motion and the restricted motions of core of star. Compared with the result of hard-sphere colloid, the crystallization process of our stars is slower. This difference could be due to the particle nature in solution, that is, our stars behave as soft sphere, while colloid particles behave as hard sphere in good solvent.

## References

[1] Zimm BH, Stockmayer WH. J Chem Phys 1949;17:1301.
[2] Daoud M, Cotton JP. J Phys (Paris) 1982;43:531.
[3] Ishizu K, Ono T, Uchida S. Macromol Chem Phys 1997;198:3255.
[4] Witten TA, Pincus PA, Catea MA. Europhys Lett 1986;2:137.
[5] Ishizu K, Ono T, Uchida S. J Colloid Interface Sci 1997;192:189.
[6] Furukawa T, Ishizu K. Macromolecules 2003;36:434.
[7] McCall DW, Douglass DC, Anderson EW. J Polym Sci, Part A 1963; 1:1709.
[8] Callaghan PT, Pinder DN. Macromolecules 1981;14:1334.
[9] Callaghan PT, Pinder DN. Macromolecules 1980;13:1085.
[10] Tanner JE. Macromolecules 1971;4:748.
[11] Tanner JE, Liu KJ, Anderson JE. Macromolecules 1971;4:586.
[12] Cosgrove T, Warren RF. Polymer 1977;18:257.
[13] von Meerwall E, Grigsby J, Tomich D, Van Antwerp R. . J Polym Sci, Polym Phys Ed 1982;20:1037.
[14] Graessley WW. J Polym Sci, Polym Phys Ed 1980;18:27.
[15] von Meerwall E, Tomich DH, Hadjichristidis N, Fetters LJ. Macromolecules 1982;15:1157.
[16] von Meerwall E, Tomich DH, Grigsby J, Pennisi RW, Fetters LJ, Hadjichristidis N. Macromolecules 1983;16:1715.
[17] Furukawa, T., Ishizu, K., J Appl Polym Sci, to be submitted.
[18] Roovers J, Martin JE. J Polym Sci, Part B: Polym Phys 1989;27:2513.
[19] Antonietti M, Gremser W, Schmidt M. Macromolecules 1990;23: 3796.
[20] de Gennes PG. Macromolecules 1976;9:587.
[21] Segre PN, Meeher SP, Pusey PN, Poon WCK. Phys Rev Lett 1995;75:958.
[22] Jian T, Anastasiadis SH, Semenov AN, Fytas G, Fleischer G, Vilesov AD. Macromolecules 1995;28:2439.
[23] Fytas G, Vlassopoulos D, Meier G, Likhtman A, Semenov AN. Phys Rev Lett 1996;76:3586.
[24] Segre PN, Pusey PN. Phys Rev Lett 1996;77:771.